Electronic Supporting Information (ESI)

Sequential double chemical activation of biochar enables the fast and high-capacity capture of tetracycline

Yuyuan Zhang,[a] Zhantu Zhang,[a] Jiayin Zheng,[a] Ruhui Peng,[a] Menglei Chang,[a] Fei Hu,[a]

Yazhuo Wang,[c] Huawen Hu[a] and Jian Zhen Ou*[b]*

[*] *Corresponding author. E-mails: huawenhu@126.com; Jianzhen.ou@rmit.edu.au*

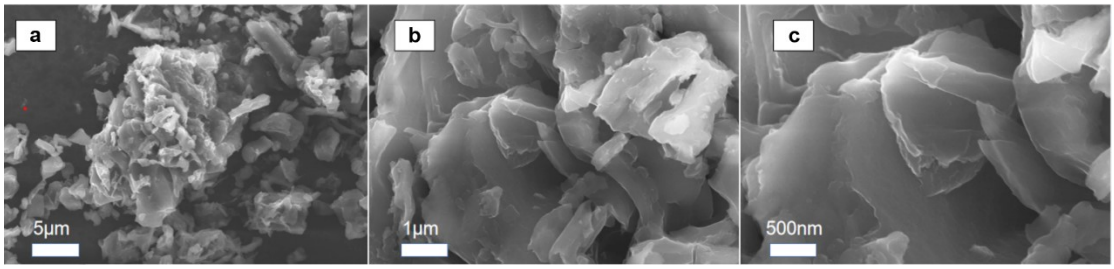

Figure S1. a-c) SEM images (at different magnification scales) of the BCM1 sample prepared by the one-step pyrolysis of dead-leaf biomass and melamine.

Table S1. Production rates calculated for the BC-K, BCM0.5-K, BCM1-K, and BCM2-K samples.

Sample	Biomass powder weight (g)	Biochar product weight (g)	Production rate (%)
BC-K	3	0.63	21.14
BCM0.5-K	3	0.85	28.50
BCM1-K	3	0.48	16.00
BCM2-K	3	0.52	17.36

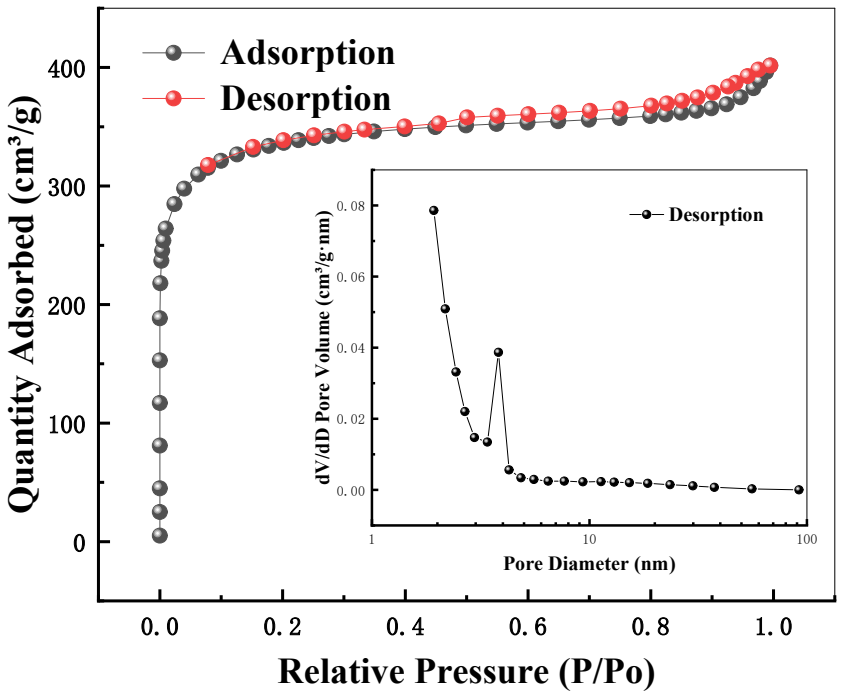

Figure S2. N_2 adsorption-desorption isotherm for the BC-K sample. Inset presents the corresponding pore diameter distribution plot.

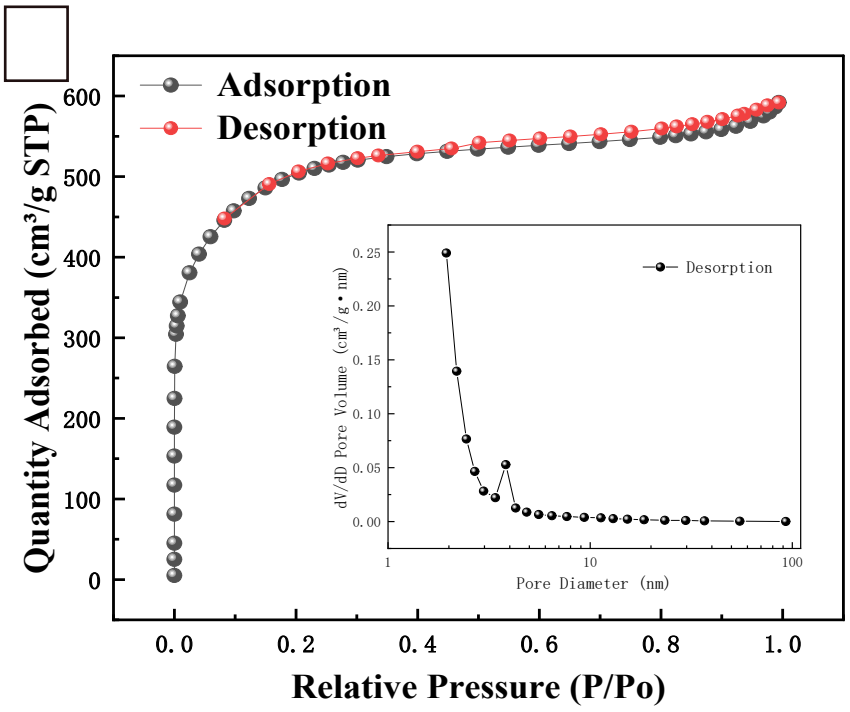

Figure S3. N_2 adsorption-desorption isotherm for the BCM0.5-K sample. Inset presents the corresponding pore diameter distribution plot.

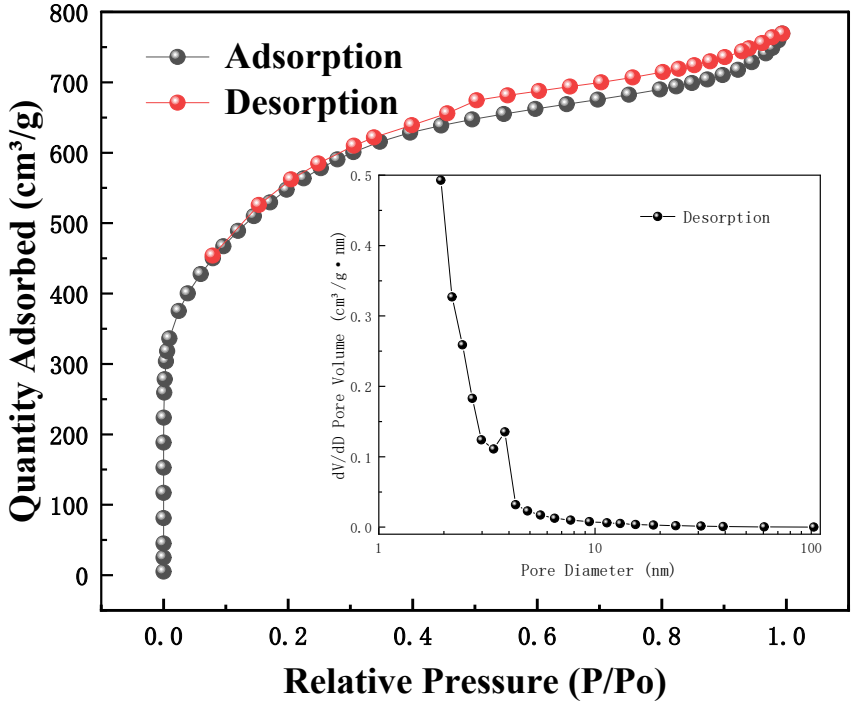

Figure S4. N_2 adsorption-desorption isotherm for the BCM1-K sample. Inset presents the corresponding pore diameter distribution plot.

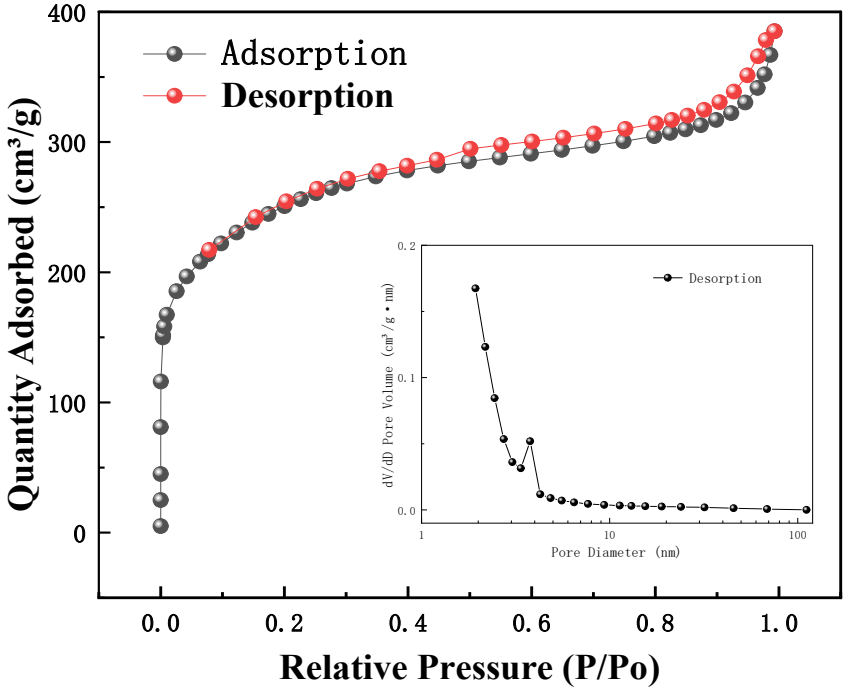

Figure S5. N_2 adsorption-desorption isotherm for the BCM2-K sample. Inset presents the corresponding pore diameter distribution plot.

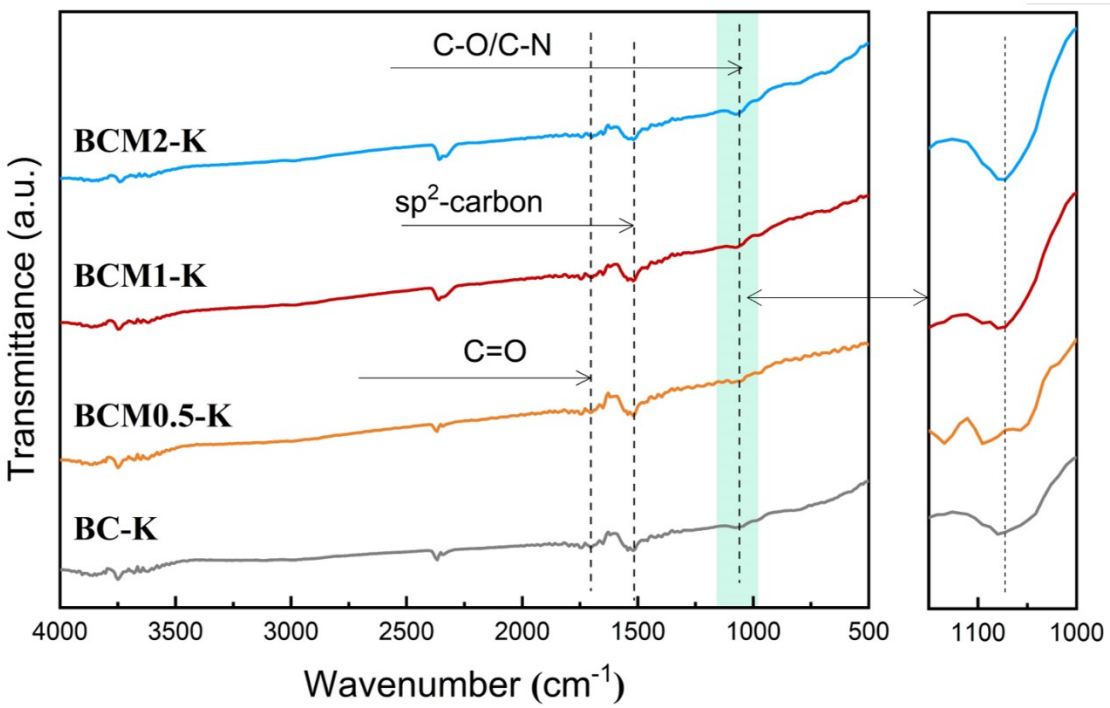

Figure S6. FTIR spectra of the BC-K, BCM0.5-K, BCM1-K, and BCM2-K samples.

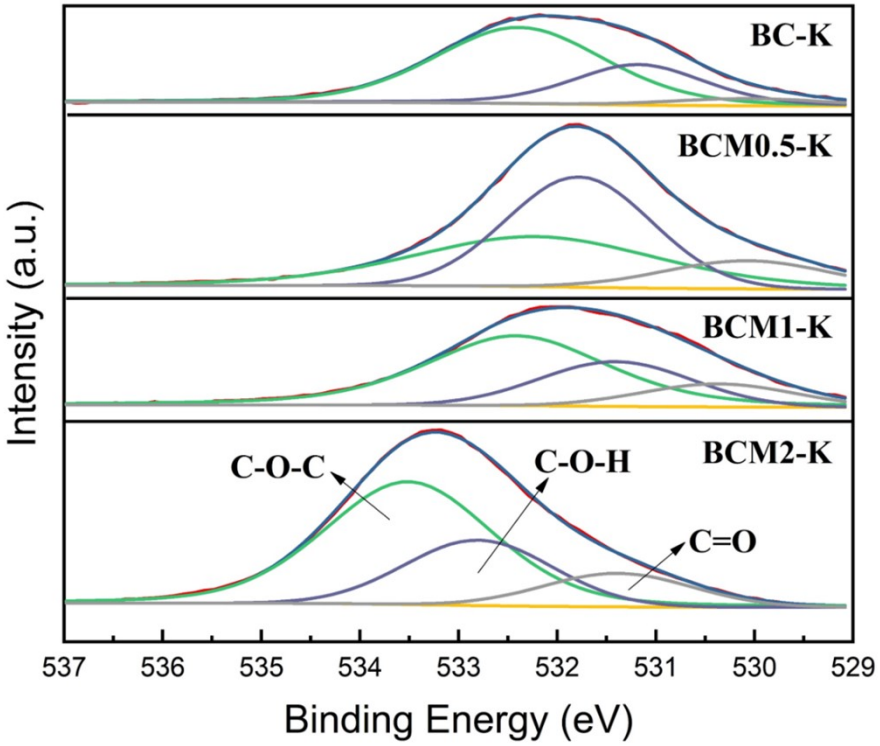

Figure S7. High-resolution XPS O1s spectra of the BC-K, BCM0.5-K, BCM1-K, and BCM2-K samples.

Table S2. Summary of the oxygen-containing functional group percentages calculated based on the high-resolution XPS O1s spectra shown in Figure S3.

Sample	Percentage of different O-containing functional groups (at.%)		
	C=O	C-O-H	C-O-C
BC-K	5.04	28.49	66.29
BCM0.5-K	13.57	40.27	46.16
BCM1-K	13.95	26.81	59.24
BCM2-K	13.27	25.70	61.03

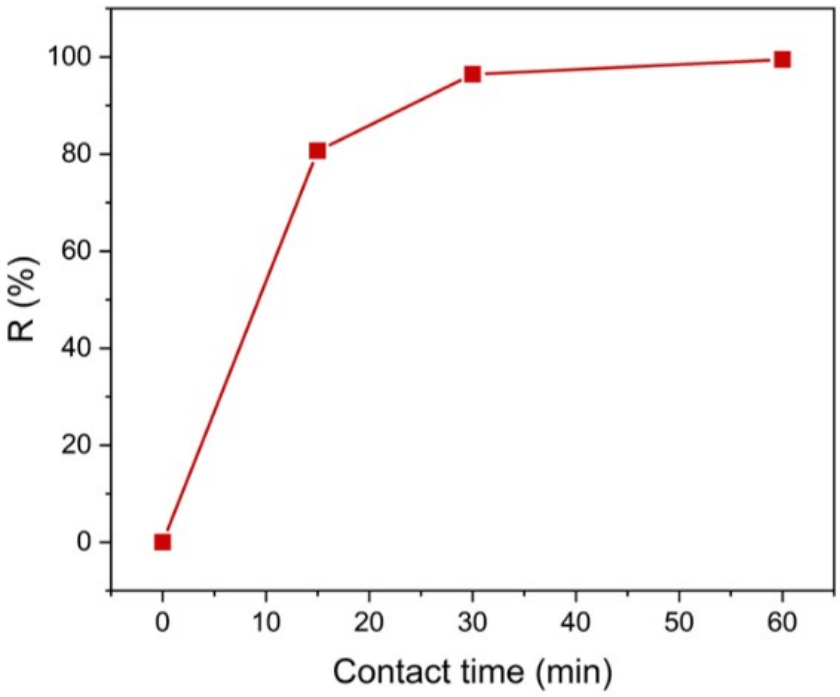

Figure S8. Investigation of contact time impact on the adsorption performance of the optimal sample (in this case, BCM1-K).

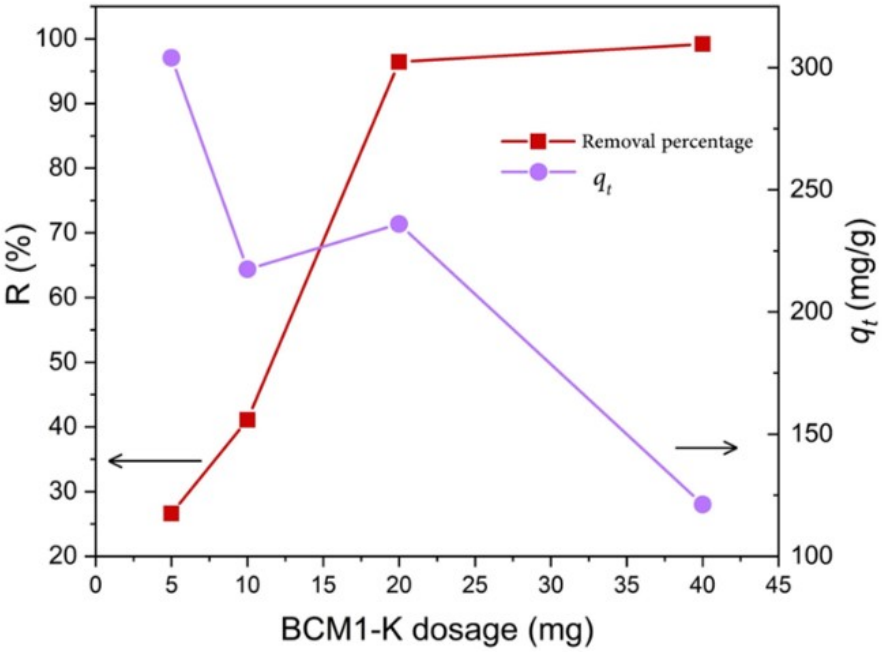

Figure S9. Investigation of BCM1-K adsorbent dosage on its adsorption performance.

Figure S10. Investigation of initial TC concentration on the adsorption performance of the optimal sample (in this case, BCM1-K).

Table S3. Comparison of the q_{max} of TC capture obtained for the optimal sample (i.e., BCM1-K) in this study with those in recent literature.

Adsorbent	Temperature (℃)	pH	q_{max} (mg/g)	Ref.
BCM1-K	**25**	**7**	**433.74**	**This work**
Magnetic chitosan	20	7	211.21	[1]
Fe_3O_4 NPs	29	7	19.6	[2]
RGO	25	7	44.23	[3]
α-Fe_2O_3/RGO	25	4	18.47	[3]
Halloysite/chitosan nanocomposite	25	8.5	15.6	[4]
Tricaprylmethylammonium chloride-conjugated chitosan hydrogel	45	7	22.42	[5]
Copper/cobalt ferrite@chitosan	25	3.5	4.48	[6]

Rice husk ash	40	5	8.37	[7]
Biochar with micropores widened by GO	40	7	336.70	[8]
Biochar co-activated by $MnCl_2$/KOH	25	7	295.98	[9]
AC	25	7	25.28	[10]
AC/Fe_3O_4/ZIF-8	25	7	57.47	[10]
Chitin/calcite composite extracted from shell waste	25	6	150.76	[11]

Note: GO, graphene oxide; RGO, reduced graphene oxide; NPs, nanoparticles; activated carbon, AC; zeolitic imidazolate framework, ZIF-8.

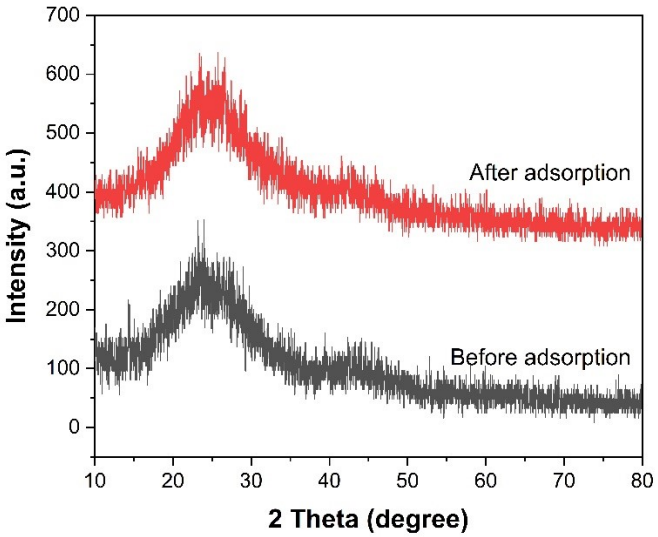

Figure 11. XRD patterns of the BCM1-K sample.

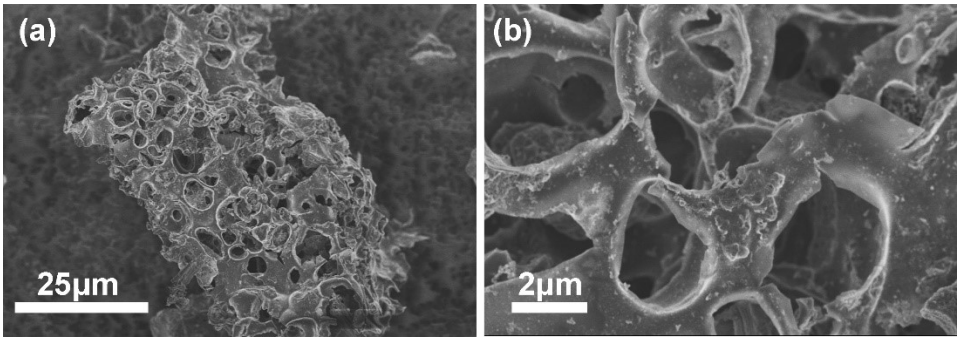

Figure 12. a,b) The morphology of the recycled BCM1-K sample. (a) and (b) are the SEM images at different magnification scales.

Figure S13. Investigation of TC solution pH on the adsorption performance of the optimal sample (in this case, BCM1-K).

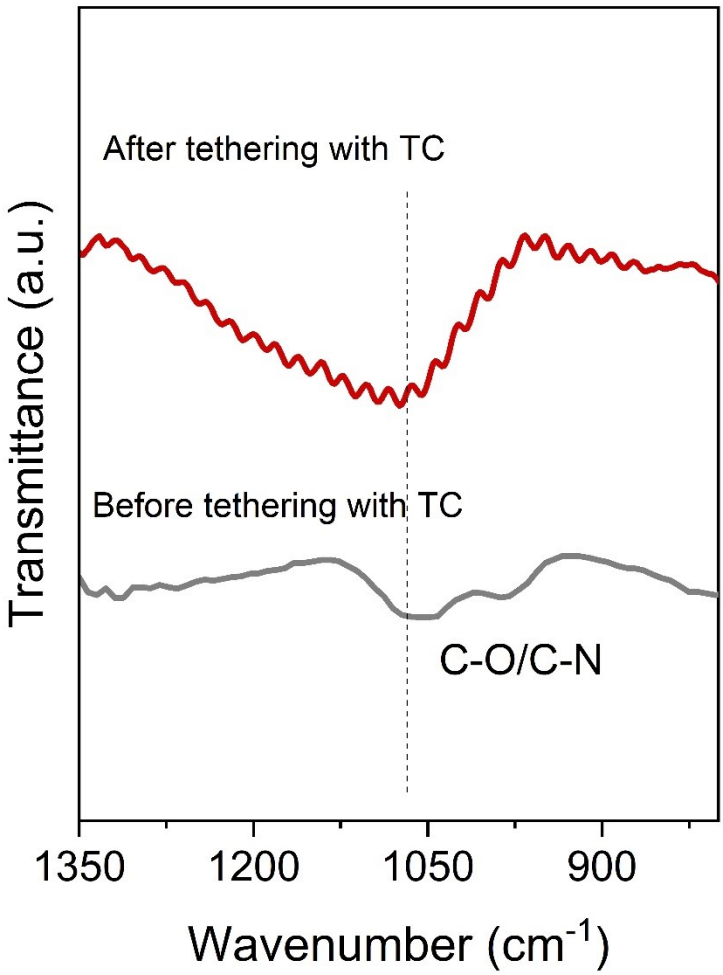

Figure S14. FTIR spectra of the BCM1-K sample before and after tethering with TC molecules.

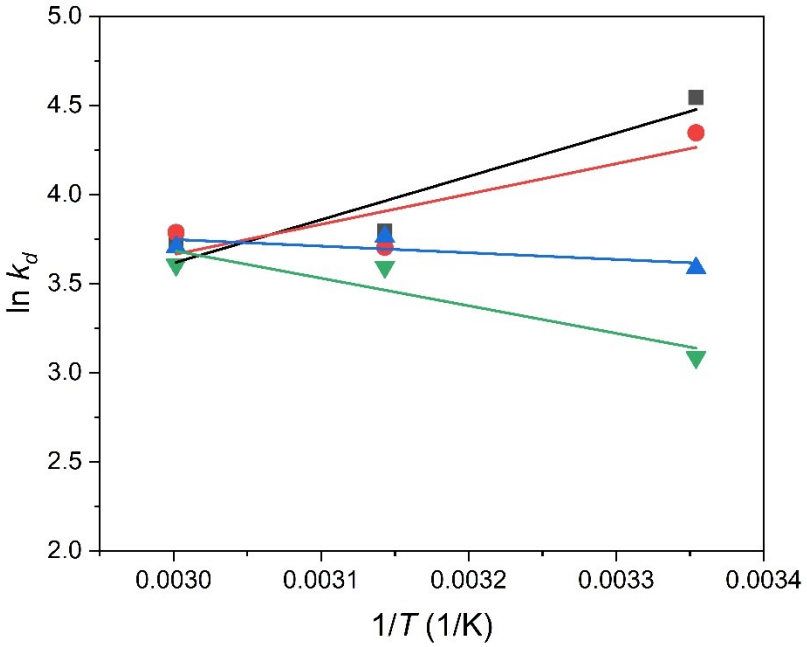

Figure S15. Van't Hoff plots of lnk_d as a function of 1/T for the adsorption system with BCM1-K.

Table S4. Summary of the thermodynamic parameters obtained via the studies of the temperature impact on the equilibrium adsorption capacities.

TC concentration (mg/L)	Thermodynamic parameters								
	ΔG^{θ} (kJ/mol)			ΔH^{Θ} (kJ/mol)			ΔS^{Θ} (J/mol K)		
	25 (℃)	45 (℃)	60 (℃)	25 (℃)	45 (℃)	60 (℃)	25 (℃)	45 (℃)	60 (℃)
50	-11.26	-10.04	-10.30		-20.22			-30.60	
60	-10.77	-9.80	-10.49		-14.13			-11.94	
70	-8.89	-9.96	-10.26		3.11			40.48	
80	-7.65	-9.50	-9.99		12.85			69.19	

References

[1] da Silva Bruckmann, F.; Schnorr, C. E.; da Rosa Salles, T.; Nunes, F. B.; Baumann, L.; Müller, E. I.; Silva, L. F. O.; Dotto, G. L.; Bohn Rhoden, C. R., Highly efficient adsorption of tetracycline using chitosan-based magnetic adsorbent. *Polymers* **2022,** *14* (22), 4854.

[2] Zhai, W.; He, J.; Han, P.; Zeng, M.; Gao, X.; He, Q., Adsorption mechanism for tetracycline onto magnetic Fe_3O_4 nanoparticles: Adsorption isotherm and dynamic behavior, location of adsorption sites and interaction bonds. *Vacuum* **2022,** *195*, 110634.

[3] Huízar-Félix, A. M.; Aguilar-Flores, C.; Martínez-de-la Cruz, A.; Barandiarán, J. M.; Sepúlveda-Guzmán, S.; Cruz-Silva, R., Removal of tetracycline pollutants by adsorption and magnetic separation using reduced graphene oxide decorated with α-Fe_2O_3 nanoparticles. *Nanomaterials* **2019,** *9* (3), 313.

[4] Erdem, S.; Öztekin, M.; Sağ Açıkel, Y., Investigation of tetracycline removal from aqueous solutions using halloysite/chitosan nanocomposites and halloysite nanotubes/alginate hydrogel beads. *Environ. Nanotechnol. Monitor. Manage.* **2021,** *16*, 100576.

[5] Ranjbari, S.; Tanhaei, B.; Ayati, A.; Khadempir, S.; Sillanpää, M., Efficient tetracycline adsorptive removal using tricaprylmethylammonium chloride conjugated chitosan hydrogel beads: Mechanism, kinetic, isotherms and thermodynamic study. *Int. J. Biol. Macromol.* **2020,** *155*, 421-429.

[6] Nasiri, A.; Rajabi, S.; Amiri, A.; Fattahizade, M.; Hasani, O.; Lalehzari, A.; Hashemi, M., Adsorption of tetracycline using $CuCoFe_2O_4$@Chitosan as a new and green magnetic nanohybrid adsorbent from aqueous solutions: Isotherm, kinetic and thermodynamic study. *Arabian Journal of Chemistry* **2022,** *15* (8), 104014.

[7] Chen, Y.; Wang, F.; Duan, L.; Yang, H.; Gao, J., Tetracycline adsorption onto rice husk ash, an agricultural waste: Its kinetic and thermodynamic studies. *J. Mol. Liq.* **2016,** *222*, 487-494.

[8] Liang, Y.; Xu, X.; Yuan, F.; Lin, Y.; Xu, Y.; Zhang, Y.; Chen, D.; Wang, W.; Hu, H.; Ou, J. Z., Graphene oxide additive-driven widening of microporous biochar for promoting water pollutant capturing. *Carbon* **2023,** *205*, 40-53.

[9] Zhang, Y.; Zhang, J.; Chen, K.; Shen, S.; Hu, H.; Chang, M.; Chen, D.; Wu, Y.; Yuan, H.; Wang, Y., Engineering banana-peel-derived biochar for the rapid adsorption of tetracycline based on double chemical activation. *Resour. Conserv. Recy.* **2023,** *190*, 106821.

[10] Tahmasebpour, R.; Peighambardoust, S. J., Decontamination of tetracycline from aqueous solution using activated carbon/Fe3O4/ZIF-8 nanocomposite adsorbent. *Sep. Purif. Technol.* **2024,** *343*, 127188.

[11] Ouyang, E.; Wu, M.; He, W.; Liu, H.; Gui, M.; Yang, H., Chitin/calcite composite extracted from shell waste as a low-cost adsorbent for removal of tetracycline and ciprofloxacin: Effects and mechanisms. *Chemosphere* **2024,** *353*, 141503.